

Infrared Reflectance of Materials at Elevated and Cryogenic Temperatures

A thesis submitted in partial fulfillment of the requirement
for the degree of Bachelor of Science in Physics from
The College of William and Mary

by

Daniel John Brooker

Accepted for Honors
(Honors, No Honors)


M. Mumtaz Qazilbash, Advisor


Hannes Schniepp


Henry Krakauer

Williamsburg, VA
April 24, 2013

Acknowledgements

I must acknowledge first and foremost the patience and guidance of my advisor Professor Mumtaz Qazilbash without whom I would have been lost countless times. I would like to thank my committee members Professors Schniepp and Krakauer. I would also like to acknowledge the graduate students who I had the pleasure of working with: Tyler Huffman for teaching me how to use the equipment in the lab and helping test the new equipment, Zhen Xing for creation of the Kramers-Kronig program for the reflectance data analysis and for helping with the testing of new equipment, and Peng Xu for coming up with the optical design that we built, and for his help in analyzing my data. I would also like to thank the undergraduates I worked with: Nick Penthorn for designing some of the components of the new vacuum chamber, and Arlo Hollingshad who along with Nick taught me how to use Solid Works for the design of all the new equipment which was built. I would like to acknowledge the William and Mary Charles Center, as well as the donors who supported my research last summer in the form of a summer fellowship which allowed me to get a jump start on this project. Lastly I must acknowledge the wonderful work of the William and Mary Machine Shop for the construction of all the parts which were made for this equipment, especially the work of John Bensele who did all of the welding which made this project possible.

Abstract

Over the past year a vacuum chamber for elevated and cryogenic temperature infrared reflectance spectroscopy was built and tested. This involved design and construction of many complex pieces of equipment which have been tested as well. The vacuum chamber has been tested and successfully holds pressures below 1×10^{-7} mbar. The temperature range has been tested for 400K to 5K. Sample positioning has been controlled to within 10 micron. This new equipment has been used to find the optical properties of various materials, for example $\text{La}_{1-x}\text{Sr}_x\text{MnO}_3$ thin films on LaAlO_3 . At cryogenic temperatures the gap structure of the incommensurate spin density wave ground state of chromium has been investigated.

Table of Contents

1) Introduction and Motivation.....	4
1.1 Introduction to Optical Spectroscopy.....	4
1.2 Experimental Goals.....	6
2) Experimental Methods.....	6
2.1 FTIR Spectroscopy.....	6
2.2 Spectroscopic Ellipsometry.....	8
2.3 Atomic Force Microscopy.....	9
3) Experimental Challenges of Cryogenic FTIR.....	10
3.1 Explanation of Experimental Requirements.....	10
3.2 Cryogenic Considerations.....	11
3.3 UHV Considerations.....	12
3.4 Optics Considerations.....	14
3.5 Repeatability Considerations.....	15
4) Results and Analysis.....	19
4.1 FTIR High Temperature Reflectance Results.....	19
4.2 Cryogenic FTIR Reflectance on chromium.....	20
4.3 Ellipsometry Results.....	22
4.3 AFM Results.....	22
5) Discussion.....	23
5.1 Introduction to Magnetic Ordering.....	23
5.2 Origins of the SDW Phase Transition.....	25
5.3 Previous Experimental Studies of chromium.....	26
5.4 Discussion of Present Results.....	27
6) Conclusion and Outlook.....	28
7) Works Cited.....	29

1) Introduction and Motivation

1.1 Introduction to Optical Spectroscopy

Optical spectroscopy is an experimental technique which uses light to probe the electronic and phonon properties of materials. This is possible if the properties of the light before and after it interacts with the sample are known. Then, since the interactions between light and matter can be analyzed according to classical electrodynamics, the electronic and phonon properties of the material can be found. This technique is very powerful because it can successfully cover a very wide range of energies, can be made very precise, and requires a relatively short amount of time to gather a large amount of information. In particular the infrared (IR) reflectance spectrum of a material is very useful for studying a wide variety of systems. From the reflectance spectrum of a material one can with some effort determine the electronic and phonon properties of a material by finding the complex dielectric function. For the many materials which have rich phase diagrams, infrared reflectance provides a useful tool for mapping the properties of these phases and their dependence on temperature, dopant levels, and external fields. We use infrared light because the energy scale of the infrared is of similar magnitude as the electronic energy scales including energy gaps which occur in insulators and ordered phases. Further, if we extend our studies into the far infrared regime we may also study the phonon characteristics of these materials.

It is very important that one be able to reach a wide range of both high and low temperatures so that one may study a much wider range of materials. This is because many of the phases which materials may enter into occur well above or below room temperature. Previously our equipment was limited to only studying the high temperature properties of materials, and we were only able to use infrared transmission. Due to the fact that many materials, including metals, superconductors, and common insulating substrates like quartz are opaque in much or all of the infrared, it is necessary to acquire the capability do reflectance as part of our infrared spectroscopic experiments. Figure 1 below illustrates this problem for the case of quartz which is opaque in part of the mid infrared spectral range.

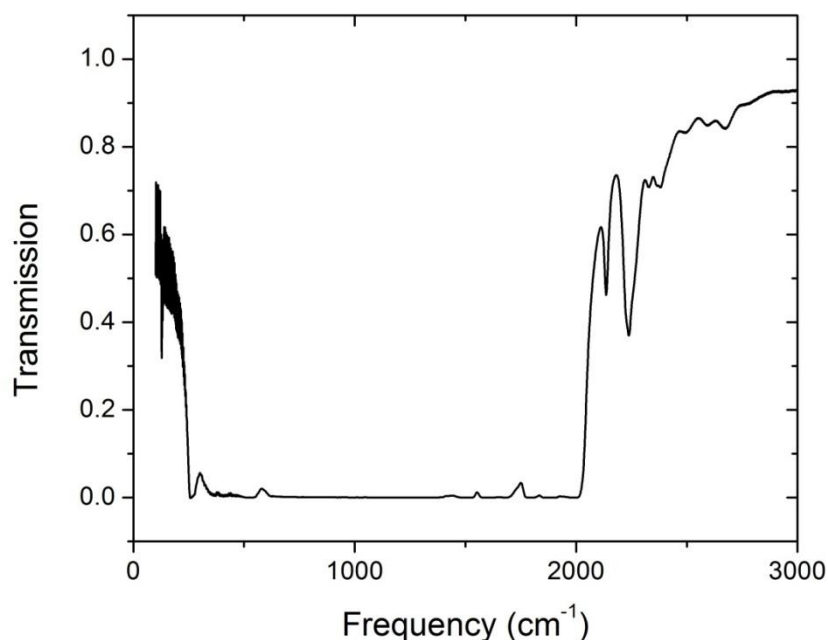


Figure 1: The transmission of a quartz substrate at various frequencies

As you can see from figure 1 above, if a material grown on quartz were to have some feature in its energy spectrum in the energy range of $200\text{-}2000\text{cm}^{-1}$ one would not be able to see the appearance of this feature against the background noise in transmission due to the very low signal caused by the opacity of the quartz substrate.

This work will detail the efforts made in the past year to achieve both high and low temperature infrared reflectance measurements. We shall begin by discussing the specific experimental apparatus which were used in this study. Then we shall take an in depth look at all of the non-trivial challenges associated with temperature dependent IR reflectance experiments. Finally we shall examine some experiments which have been conducted at both high and low temperatures using the new reflectance equipment which was built. In the case of room temperature and cryogenic reflectance we shall examine chromium (Cr), a metal which exhibits interesting gap-like features in the infrared due to a spin density wave (SDW) phase transition.

1.2 Experimental Goals

We want to be able to perform high temperature infrared reflectance measurements up to 400 K. At elevated temperatures we have studied, for example, a metal-insulator transition (MIT) in $\text{La}_{0.67}\text{Sr}_{0.33}\text{MnO}_3$ (LSMO) grown as a thin film on a LaAlO_3 (LAO) substrate. This was done using the infrared reflectance setup in the mid- and far-infrared between 300K and 400K. In the low temperature regime, we will examine the complex dielectric function of chromium across the IR as well as the ultraviolet (UV) and visible. Due to the fact that past work in chromium has been inconsistent on the number of gaps we hope to shed light on this confusion, and provide some closure to these unanswered questions about the properties of chromium. We will do this by measuring the temperature dependent complex dielectric function of chromium in the mid-infrared down to cryogenic temperatures well below room temperature. We will also measure the complex dielectric function into the visible and UV spectrum at room temperature. In our chromium experiment we will compare our data with that of past results in the IR¹, and in the ultraviolet and visible range^{2,3}. In the next two sections we will discuss the specific experimental techniques used in this study to measure these properties of chromium.

2. Experimental Techniques

In this project, my goal was to develop equipment to map the complex dielectric function $\epsilon(\omega)$ across a wide range of frequencies. The complex dielectric function is an equivalent set of information to the complex index of refraction or the complex conductivity. This set of information completely describes the optical properties of a material as a function of frequency. In our experiment we want to cover the range of infrared to ultraviolet light frequencies. This range will typically correspond to electronic features associated with metallic conduction and energy gaps within a material. To do this I used two different techniques: FTIR reflectance spectroscopy and spectroscopic ellipsometry. Further, to aid in the modeling of our sample I mapped the surface topology of the sample using an atomic force microscope (AFM). We will now discuss how each of the methods used in this study may yield the

complex dielectric function, or the complex optical conductivity.

2.1 FTIR Spectroscopy

FTIR is an experimental technique which is short for Fourier Transform Infrared Spectroscopy. In this technique broadband infrared light is used with a type of Michelson interferometer where one of the arms has a variable length to generate an interference pattern. This is accomplished by putting one of the mirrors on a motor and having it move back and forth. The light is then either transmitted through or reflected off a sample and into a detector. The detector measures the intensity spectrogram of the light as a function of mirror position and the wavelength of the light source. Each mirror position will cause a different wavelength of light to interfere constructively. The detector sees all of these interference patterns superimposed. Then, knowing the mirror velocity, a fast Fourier transform is performed to get the intensity as a function of wavelength. This can then be normalized to a reference sample to give the reflectance or transmission of a sample. FTIR Spectrometry is useful for several reasons, namely being: It is fast, it has high precision, and it is broadband. In this experiment a Bruker Vertex 80v vacuum spectrometer was the FTIR Spectrometer used. Figure 1 below shows its optical arrangement.

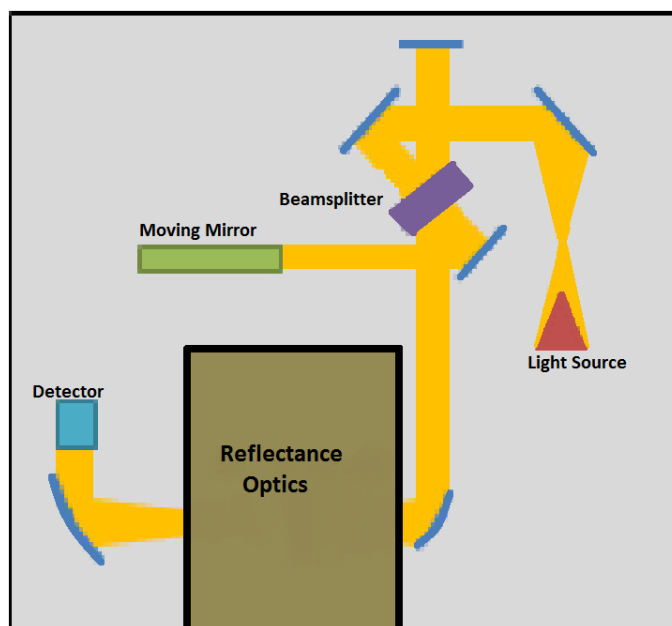


Figure 1: The beam path of an FTIR Spectrometer. (Note: The Section labeled Reflectance will be discussed and shown in section 3.4)

Since FTIR is a broadband measurement the spectral range covers the entire IR spectrum from the THz into the visible (2 meV to 2.5 eV). These energies allow one to observe a wide range of phenomena including: band gaps, energy gaps due to phase transition, and optical phonon modes. Since the energy gaps we are searching for as outlined in section 1.4 occur at low temperatures, the reflectance measurements must be performed at cryogenic temperatures. This means our FTIR sample chamber will have to be cryogenic, the full implications of which will be discussed in section 3. Yet another challenge of FTIR is that it measures broadband reflectance intensity only which needs to be analyzed to obtain the complex dielectric function. This is in contrast to ellipsometry which directly measures both parts of the complex optical constants for every frequency. Fortunately infrared reflectance data can be analyzed together with the ellipsometry data at higher frequencies to obtain the infrared complex dielectric function either by using the Kramers-Kronig relations to give the phase shift of the infrared reflectance⁴, or by fitting the reflectance and ellipsometric data with Kramers-Kronig consistent oscillators.

2.2 Spectroscopic Ellipsometry

Ellipsometry is an experimental technique which one can use to find the optical constants of a material across a broad range of frequencies. In our lab we use a Woollam Variable Angle Spectroscopic Ellipsometer (VASE) which covers a range from 0.6-6eV. Ellipsometry directly measures the change in polarization of light after reflection off of a sample. The initial polarization state of the light is known to be linear, and after reflection off a sample at some known angle the polarization will be elliptical. The detector directly measures Ψ , which is tilt of the ellipse, and Δ , which is the phase difference between the s- and p-polarized light i.e. the eccentricity of the ellipse. These two ellipsometric coefficients together describe the polarization ellipse completely. They are related to the optical constants via the Fresnel reflection coefficients which are related to Ψ and Δ by

the following equation.

$$\frac{\tilde{r}_p}{\tilde{r}_s} = \tan \Psi e^{i\Delta} \quad (1)$$

By measuring both Ψ and Δ across a broad range of frequencies one can calculate directly the optical constants of a material. Shown below in figure 4 is a diagram demonstrating what Ψ and Δ correspond with physically.

Due to the fact that our measurements are optical in nature, the reflections off our sample will have some scattering if the surface roughness is on the same order of magnitude as the wavelength of light being used to probe the sample. For the short wavelengths of the VASE this is $\sim 200\text{nm}$. In order to determine the surface roughness directly so as to include it in the model we measured the surface topography directly using atomic force microscopy AFM.

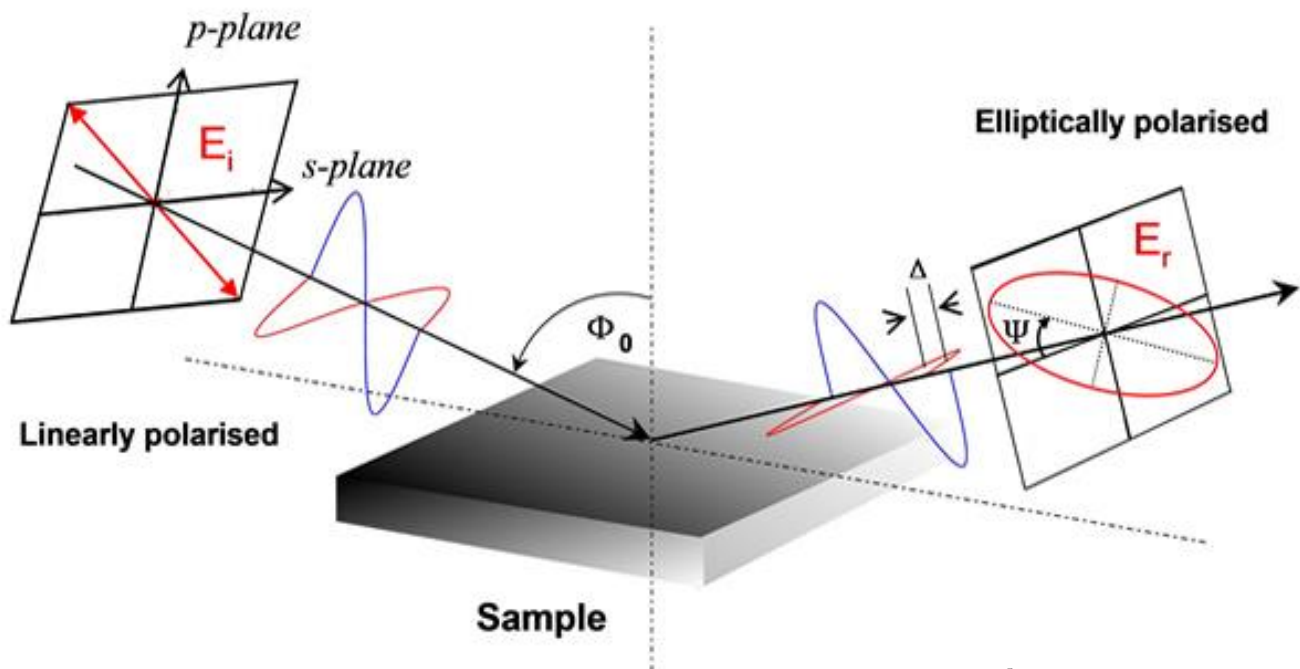


Figure 2: An illustration of the ellipsometric coefficients Ψ and Δ ⁵.

2.3 Atomic Force Microscopy

Atomic force microscopy is a technique which can be used to obtain the surface roughness of a material. In our lab we use an AFM from Neaspec. The basic principle behind an AFM is that when a very small cantilever is scanned over a very near surface it will deform due to the atomic forces

between the cantilever tip and the surface. The tip oscillates up and down over the surface, and a feedback loop is made so that the amplitude of these oscillations stays constant. By measuring the voltage required to maintain these oscillations one can calculate the distance between the tip and the surface. By scanning over the surface one can establish what the topography is by observing the characteristic heights of both peaks and valleys on the surface of a sample. Knowing this roughness allows one to further characterize spectroscopic data which is taken at wavelengths which may be on the same order as the surface roughness.

3. Experimental Challenges of Cryogenic FTIR

3.1 Explanation of Experimental Requirements

There were several design challenges which had to be met in order for this project to succeed. We will consider all of them individually and discuss how they were specifically addressed here. These included:

- **Cryogenic and high temperature requirements-** In order to study various condensed matter systems it is necessary to achieve stable temperature control from as low as 4K up to 400K with the ability to take data at any temperature in between.

- ✦ **Ultra- high vacuum (UHV) requirements-** In order to avoid ice formation on samples the pressure must be $\sim 1 \times 10^{-7}$ mbar or lower. This will prevent the formation of ice crystals on the sample for the duration of the experiment. To achieve this vacuum requires a specific type of welding using stainless steel, as well as specific types of ultra-high vacuum (UHV) compatible ports on the chamber. This also requires the custom design of infrared windows and an electrical feed through which are UHV compatible.

- ✦ **Constraints on optics-** Making all of the optics fit in the existing FTIR chamber was difficult for several reasons. In particular the optics of the commercial spectrometer has a fixed input and output in the form of a parabolic and an ellipsoidal mirror which have fixed focal lengths and positions. One

must also try to minimize the number of mirrors used since there is a small absorption loss on each reflection, which compounds as the number of mirrors increase.

⤴ **Repeatability requirements-** The experiment needs to be accurately reproducible which requires fine control on the sample location. In order to normalize any geometric effects out of the data the reflectance measurements at all temperatures will be taken twice, the latter performed with the sample coated in gold *in situ*. The experimental measurement itself involves measuring the reflectance of the sample, of an aluminum or gold reference mirror, and then dividing the two. Thus the sample must be able to change position requiring fine positioning to within a few micrometers.

In the past year all of these challenges were addressed as the entire assembly was built and vacuum tested, the cryogenic capabilities were established, a computer program was written for controlling sample motion, and the optical design was completed. We will now discuss the specifics of how all of the problems were addressed in turn.

3.2 Cryogenic considerations:

⤵ The cryostat itself is an ARS cryostat which is cooled using liquid helium. The evaporation temperature of liquid helium at atmospheric pressure is 4.2 K; however with the use of evaporative cooling which involves pumping on the exhaust gas with a vacuum pump, we can achieve temperatures below this. The temperature is measured on the sample mount, which is at the end of the cold finger. It is protected from external radiation by the heat shield which is nickel-plated high purity copper. There is also a heater which along with helium flow can be adjusted to control the temperature of the sample. A picture of the cryostat itself is below in figure 3 with all important features labeled.

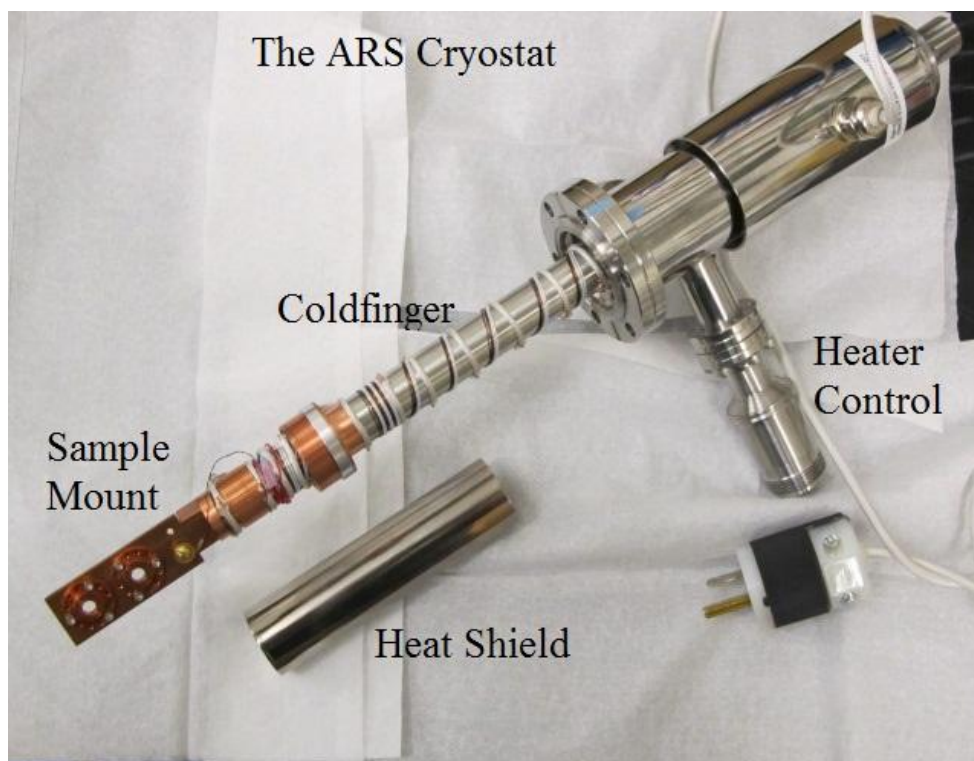


Figure 3: The cryostat with cold-finger, sample mount, and heater control labeled.

3.3 UHV Considerations:

The chamber was designed to be welded on to a plate which would attach to the front of the sample chamber of a Bruker Vertex 80v FTIR spectrometer. The chamber itself is rectangular and measures 160mm x 85mm x 57mm. Since the desired pressure was below 10^{-7} mbar the chamber had to be made of stainless steel, and the welds had to be UHV compatible. To ensure this all welds were tested using a helium mass spectrometer leak detector. Further all ports into the chamber must be UHV ports, meaning that they seal using stainless steel conflat. These conflat have a circular knife-edge which presses into a gasket of either copper or rubber. When the gasket is compressed a seal is formed. There are five UHV ports into the chamber. They are: an optical port, an electrical feed-through, a port for the sample, a port for the pump, and a port for the pressure gauge. Pictures of the various pieces of equipment and the chamber as they are constructed and assembled are shown below in figure 4.

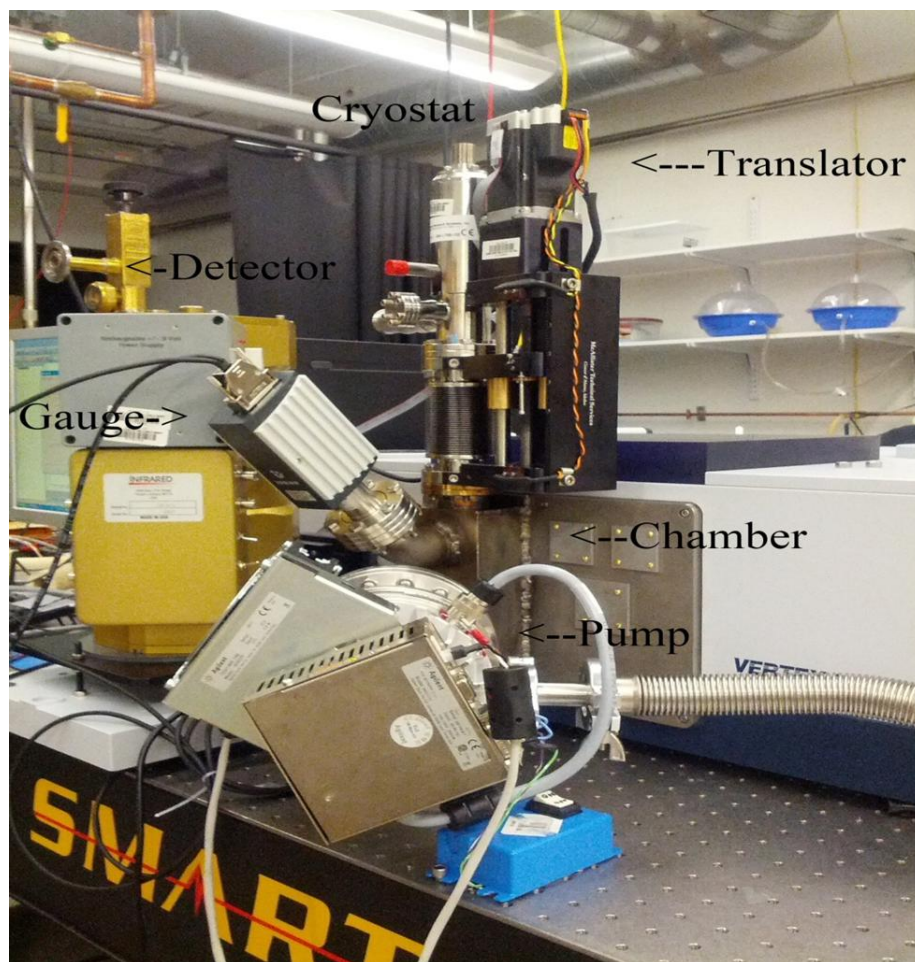


Figure 4: The vacuum chamber as assembled with all visible parts labeled. Not shown: optics, optical window, electrical feed-through

The sample is mounted to an ARS cryostat which is moved vertically using a McAllister translator with a programmable micro-step motor. The vacuum chamber has been tested successfully and has achieved a vacuum of 2.77×10^{-8} mbar at room temperature. This test included along with the chamber, all UHV components such as the cryostat, and evaporator.

The optical window design itself was also challenging, and serves as a potential limit on ultimate pressure achieved if there are leaks. The window must be thick enough to withstand a pressure differential of 1atm so that the UHV chamber can be in vacuum while the FTIR side is at ambient pressure, and yet it must be thin enough so as to minimize losses due to absorption. The window itself must be secured to a UHV conflat, and in order to make such a seal vacuum tight a UHV compatible

adhesive must be used. Two windows were built; one of the windows is potassium bromide (KBr) which has high mid infrared and near-infrared transmission. The other is polypropylene which has good far infrared transmission. The polypropylene sheet was especially thin being only 0.003” thick. To minimize strain on polypropylene sample a slotted window was designed as opposed to the circular KBr window. Since the window is slotted the strain depends mostly on the width of the window, its smaller dimension, and not so much on its length⁶. Shown below in figure 5 is a picture of the two windows as constructed. The two windows have both been successfully tested and can hold UHV pressures.

3.4 Optics Considerations:

The optics design was particularly difficult for the following reason. Outside of the chamber the final mirrors and the positions of the detectors are fixed. In particular there is an ellipsoidal mirror which focuses light from a specific point in the chamber onto the detector. This point would normally serve as a focus of the light and as the sample position in transmission measurements. The output beam after reflectance from the sample must also have its focus there. To do this required the use of three conic mirrors, two parabolic the other spherical. Moreover it must be ensured that the beam's real focal size, which is not



Figure 5: Left, the polypropylene window. Right, the KBr window.

an ideal point in space is as small as possible. To do this an aperture will be placed at a focal point of

the light before the sample this is because for larger samples we would like that the spot be smaller than the sample diameter. In practice the spot size is ~2mm. Finally the entire optical design must be easily removable, to make it simple to switch between reflectance and transmission set ups. This was achieved by constructing the entire apparatus on a miniature optical breadboard which is itself mounted into the FTIR chamber. Below is a sketch of the final beam path to be used in reflection experiments followed by a picture of the optics as constructed.

3.5 Repeatability considerations:

The McAllister translator is used to move the sample and reference mirrors into the center of the beam path, and to move the sample in line with the gold evaporator. The accuracy of this translator depends on the motor's ability to check where the translator is. Normally the motor would simply count the number of motor steps it takes. However when the motor is under a load, such as the load of the cryostat, the motor may not step and stall on the drive shaft which actually moves the cryostat, causing the number of motor steps to no longer reflect the distance that the translator has traveled. This error would make it impossible for the sample motion to have repeatability of the order of micrometers which is why it is necessary to use an encoder along with the motor. The encoder counts the number of steps the translator actually takes and compares it with the number of steps the motor takes. This is what allows us to have the required accuracy. The motor was programmed using the existing M-Code

software which came with the motor. Since the software contains language to construct both if statements and go-to statements it is possible to construct complete loops within the motor programs.

An example of such a program that might be used in this application is as follows:

- ⤴ Move the translator to a specified position.
- ⤴ Is the translator at specified position according to the encoder?
 - If yes: Stop program
 - If no: Go to the beginning of the program

The specific positions which place either the sample or reference in the center of the beam path are not preset positions, but rather are calibrated from the amount by which the cryostat shrinks or expands along with a known room temperature position. Thus, the position which the translator must move to will ultimately be a function of temperature, which will be a user input variable in the final program. This input variable will be put into a simple linear equation which is fit to a measured contraction coefficient for the cryostat's cold finger. Such a formula might appear as follows:

$$(\text{Position}) = (\text{Room Temp Position}) (297 - \text{Temp}) (\text{Contraction Coefficient}) \quad (2)$$

Once this contraction is found the algorithm for a program which moves the sample into the center of the beam path will be as follows:

- ⤴ Prompt user for temperature in Kelvin
- ⤴ Calculate required sample position using (2)
- ⤴ Move the translator to a specified position.
- ⤴ Is the translator at specified position according to the encoder?
 - ⤴ If yes: Stop program
 - ⤴ If no: Go to the beginning of the program

In order to normalize a large sample such as the Cr sample used in this experiment one must have a material which has a smooth and high reflectance curve that one can compare to. In the infrared

two such materials one can use are either gold or aluminum. In this experiment we will reference the sample with gold. This will be done by evaporating gold on to a glass slide *in situ*. This glass slide coated with gold will be used as a reference mirror. In order for the reference to be adequate the gold must be evaporated in a thick enough layer so that there are no thin film effects.

Further the reference itself must be aligned relative to the sample so that it will also reflect the beam into the detector. This is accomplished using an external alignment set-up designed to have the same angle of incidence as the reflectance chamber. This was done by holding a small laser pointer at a fixed angle with a fixed aperture and target. The laser reflects off the sample and travels through the aperture onto the target. The cryostat is then moved so that the reference mirror is in the laser path. If the laser follows the same path that it did when reflecting off the sample then the two have the same relative alignment. Figure 8 shows the external alignment set-up as constructed.

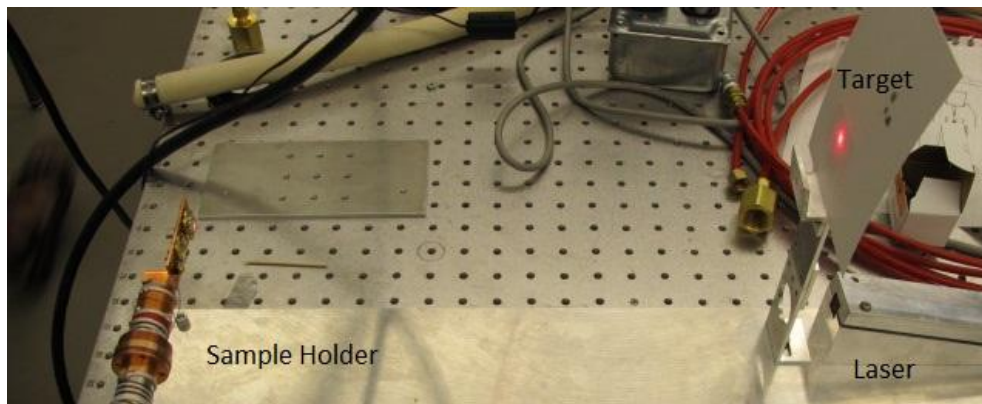


Figure 8: The external alignment with laser, sample, and target shown

An evaporator may be used to evaporate gold on to a sample *in situ* after the reflectance of the sample has been measured at all temperatures with respect to a reference. This is necessary when the sample size is smaller than the spot size of the incident light. The evaporator consists of a UHV electrical feed through which has been welded to a 1.33” stainless steel con-flat flange. Attached to two of the wires are brass end caps with mounts for a fine tungsten wire. The tungsten is heated using a programmable DC power supply and a current of 2 amps. Around the tungsten will be wrapped small loops of gold

which will be heated to evaporation. The vapor pressure of gold at 1×10^{-7} mbar is about 1250K^7 . This means that with current attainable vacuum heating the tungsten wire to a temperature of 1250K will be more than suitable for gold evaporation. The gold particles will then coat the sample, and a protective shroud will prevent gold from contaminating the rest of the chamber. Seen below is a picture of the gold evaporator as assembled with relevant parts labeled.

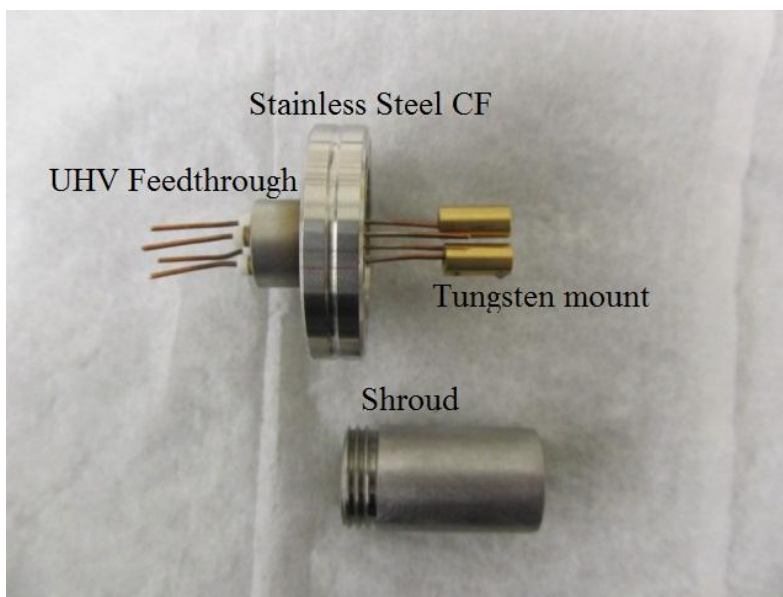


Figure9: A picture of the evaporator as constructed with feed-through, conflat flange, tungsten mount, and shroud noted.

Now that we have discussed the specifics of how addressed all the challenges behind making a low temperature FTIR measurements we will discuss the results. We will begin by discussing the ellipsometry and AFM data which were used to characterize the chromium sample, and then we will discuss the results of the cryogenic FTIR reflectance measurements.

4 Results and Analysis

4.1 FTIR High Temperature Reflectance Results

The FTIR Reflectance set up that was discussed in Section 3 was used to measure the reflectance at high temperature of $\text{La}_{0.7}\text{Sr}_{0.3}\text{MnO}_3$ samples grown on lanthanum aluminate. Figure 10 below shows representative results that were obtained for high temperatures.

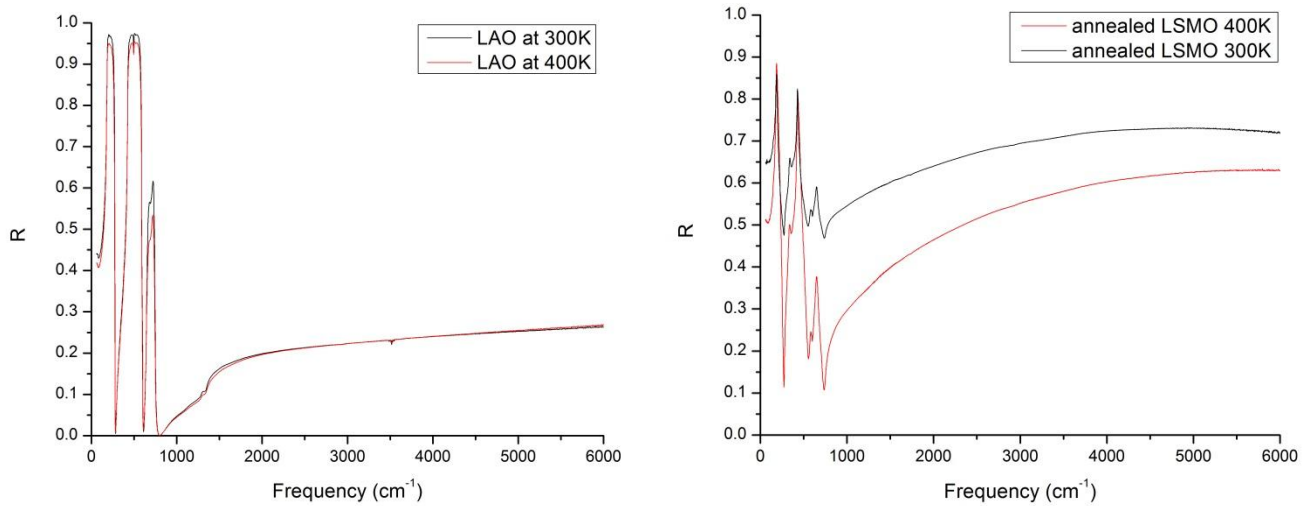


Figure 10: Room temperature and high temperature reflectance data taken for Left: an LAO substrate, Right: Annealed LSMO film on LAO

As can be seen above the LAO shows no large differences in reflectance at high temperature. The features below 1000cm^{-1} on either graph are infrared active phonons from the substrate. However one can also see immediately that the LSMO has temperature dependence in the reflectance whereas the LAO does not. This is a feature of the metal insulator transition in LSMO in this temperature range.

4.2 Cryogenic FTIR on chromium

At low temperatures our FTIR reflectance unit was used to measure the reflectance of chromium which undergoes a spin density wave (SDW) phase transition below $T_N=311\text{K}$ ⁸. The results for the low temperature reflectance of chromium are showed below in figure 11 for the MIR. The data has been normalized with that of 400K Cr so as to compare with past results¹. In terms of reflectance data the main effect of the SDW transition is to cause the opening of gaps in the MIR reflectance spectrum. There has however been debate as to the number of gaps with anywhere from 1-3 temperature dependent features being observed⁸. Section 5 will contain a discussion of the SDW transition in chromium as well as some history of the past IR spectroscopy work done on chromium. Figures 11 and 12 below show the absolute reflectance and the reflectance ratio, which is obtained

when the absolute reflectance data is divided by the reflectance spectrum of 400K paramagnetic chromium. Three gaps are observed from the absolute reflectance when compared with the room temperature results. The reflectance ratio is compared with past data below as well.

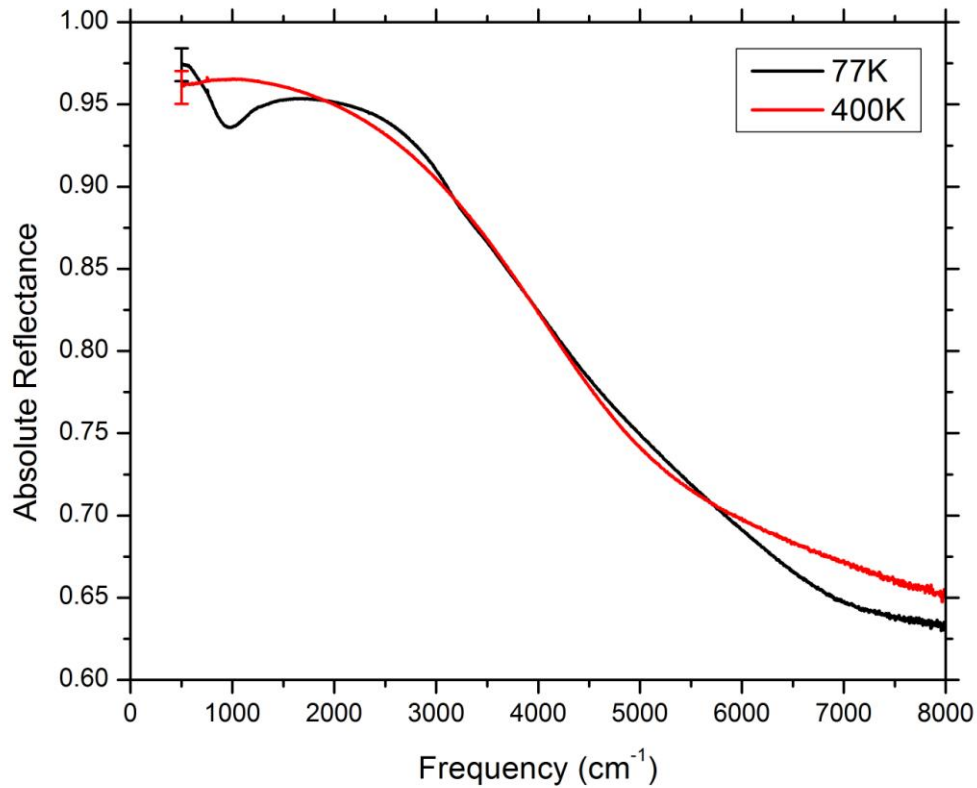
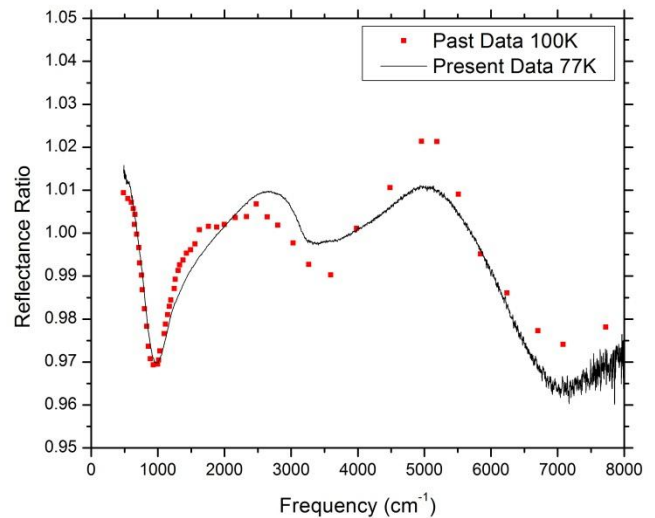
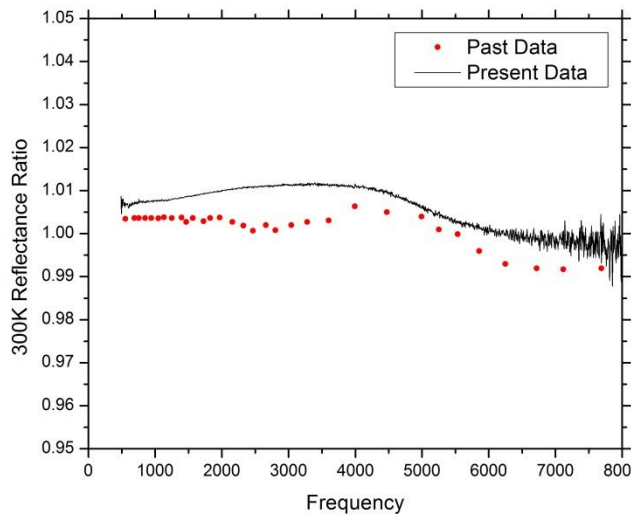


Figure 11 (Above): The absolute reflectance of chromium at 400K and 77K

Figure 12 (Below): The reflectance ratio of chromium at 300K and at low temperature compared with past data¹



4.3 Ellipsometry results

Shown below in figure 12 are the results of our ellipsometry measurements from 0.6eV to 6eV at room temperature compared with prior experiments^{2,3}. In general our data fits remarkably well. The only thing of note is that both our data and the data of Romaniello *et.al.*³ departs from that of Nestell and Christy² at low frequencies in spite of agreeing well on the whole.

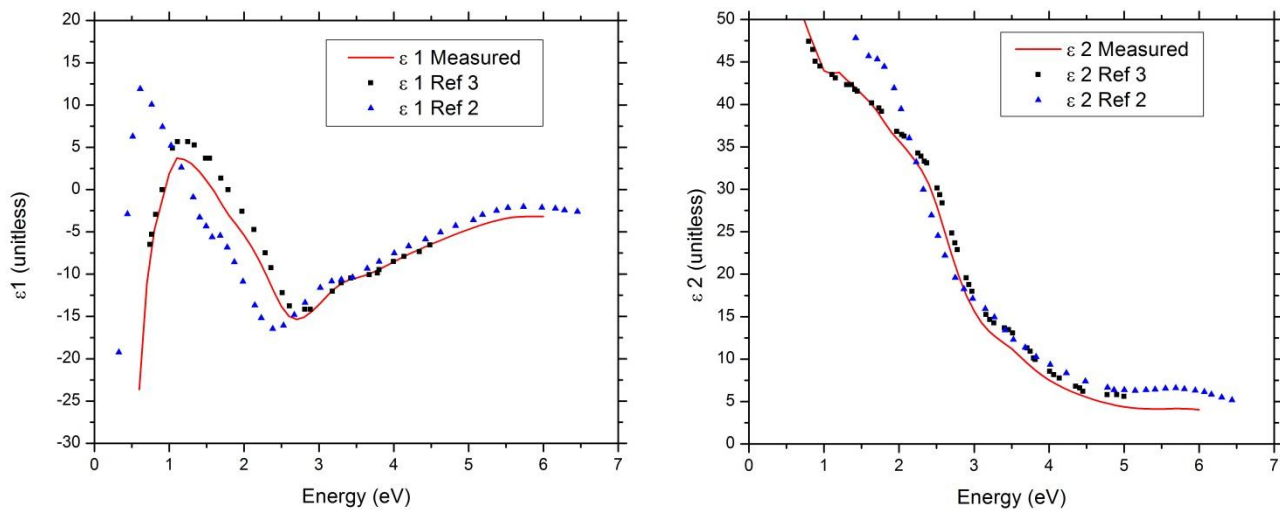


Figure 12: ϵ_1 and ϵ_2 as found by ellipsometry in the range of 0.6-6eV. The data has been compared with that of past studies^{2,3}

4.4 AFM Results

The AFM data was used to characterize the sample roughness of the chromium. This was done by measuring the required piezo voltage to keep the AFM tip oscillating at constant frequency as a function of position over the sample. A $4\mu\text{m} \times 4\mu\text{m}$ grid of the sample was measured. It was ensured that there were no large dust particles on the sample so as to ensure that our characteristic roughness accurately reflected that of the sample. Figure 13 below shows a 2D map of a section of the measured surface.

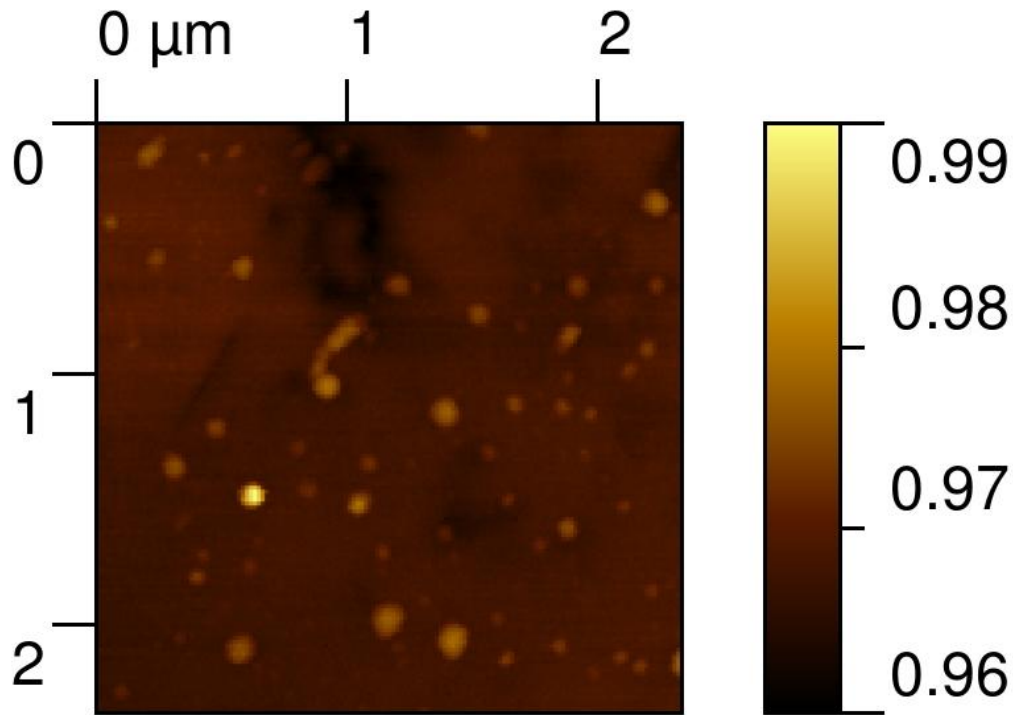


Figure 13: A 2.5x2.5 μm grid showing the measured sample roughness

The scale of figure 13 is shown in terms of a height scale which has been adjusted so that 1 unit of height is 1 μm . Therefore one can see that according to figure 11 the peak to peak roughness in this region is ~ 10 nm. This is important for the ellipsometry results because it implies that the ellipsometry data is not affected by the surface quality since the UV wavelengths are ~ 200 nm and the roughness is much smaller than this.

5 Discussion

In this section we will begin by examining some theory of the SDW phase transition in chromium, as well as past results for optical spectroscopy on chromium at low temperatures. We will then look at interpreting the results of sections 4.2-4.4.

5.1 Introduction to Magnetic Ordering

Magnetic ordering in metals arises as the ground state in systems wherein it is energetically favorable at low temperature for the electron spins to transition to an ordered state. Two well know situations for this ordering are ferromagnetism and antiferromagnetism. Figure 14 shows a

visualization of these simple types of magnetic ordering as well as a system with no ordering for reference.

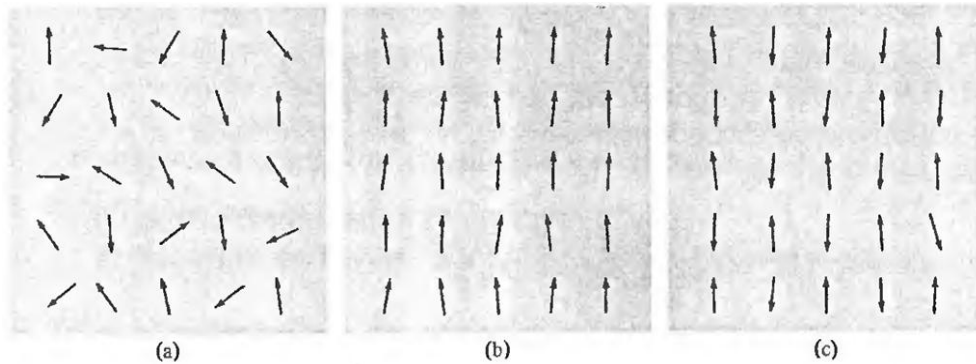


Figure 14: A) A simple paramagnet, B) A simple ferromagnet, C) A simple Antiferromagnet⁹

In contrast to the above examples chromium exhibits a more complex form of magnetic ordering. chromium, a bcc metal, exhibits a type of antiferromagnetism which is called a spin density wave (SDW). We may define the spin density of a material along a given axis x as:

$$S_z(x) = 1/2 (n_{\uparrow}(x) - n_{\downarrow}(x)) \quad (3)$$

where the subscript z refers to the fact that we are looking at the z component of electron spin, and n are the densities of spin up and spin down electrons as a function of position x . We may say that chromium has an antiferromagnetic ground state because the integral of the spin density along any cubic axis is 0; however, for the SDW in chromium the spin density is a sinusoidally varying wave in space. Moreover the wave is incommensurate with the lattice periodicity meaning that the wavelength of the SDW is not a multiple of the lattice size. A visualization of this type of ordering is shown below in figure 15.



Figure 15: A visualization of how the electron spins order themselves spatially in Chromium⁹

This transition which occurs at a critical temperature $T_N=311^8$, gives chromium all of its unique properties at low temperatures. We will now consider a brief theoretical overview of why this ordering happens, and then we will discuss the previous optical experiments which have been done on chromium and their findings.

5.2 Origins of the SDW Phase Transition

The origins of the SDW in chromium may ultimately be traced back to instabilities in the Fermi surface of chromium. Before we may examine this let us first examine the Fermi surface of a one dimensional electron gas. In this simplest case the Fermi surface is simply two points in phase space at $\pm k_F$. One may then consider the susceptibility of this 1D material to external perturbations. The susceptibility is defined as the amount of charge which is induced at a location due to the presence of a field at some other location. It is given for the 1D electron at $T=0$ gas by:

$$\chi(\vec{q}) = \int \frac{d\vec{k}}{2\pi} \frac{f_k - f_{k+q}}{\epsilon_k - \epsilon_{k+q}} (4)$$

Where \vec{q} is the separation vector in phase space, f is the Fermi function, and ϵ is the energy. The solution to this integral is given by:

$$\chi(q) = \frac{-e^2}{\pi \hbar v_F} \ln \left| \frac{q+2k_F}{q-2k_F} \right| (5)$$

where again q is a separation in phase space. From this solution it is quite obvious that there will be divergent charge redistribution in the material at the Fermi surface for any small perturbation. Alternatively we may say that the surface is instable in the paramagnetic state. Oddly enough however this instability does not generally occur in the two or three dimensional electron gas¹⁰. It would seem that only surfaces which exhibit ‘nesting’, which is to say surfaces with the same shape which are separated by some vector in phase space, contribute to the divergence of this integral.

In the case of chromium it was Lomer¹⁰ who first attributed the SDW transition to nesting in the Fermi surface of chromium. Figure 16 shows a section of the Fermi surface of chromium with nesting

vectors highlighted. In the case of chromium the two surfaces which nest to create the SDW instability are hole and electron surfaces in the Fermi surface separated by $k = \frac{2\pi}{a}(1,0,0)$. An interesting feature to note is that the nesting in chromium is imperfect nesting in the sense that the surfaces are not exactly the same size. Moreover because Q is not a multiple of the reciprocal lattice size the SDW is incommensurate. However, if the electron and hole surfaces were the same size then the nesting would be perfect and if the wave vector Q were a multiple of the reciprocal lattice size the SDW would be commensurate¹².

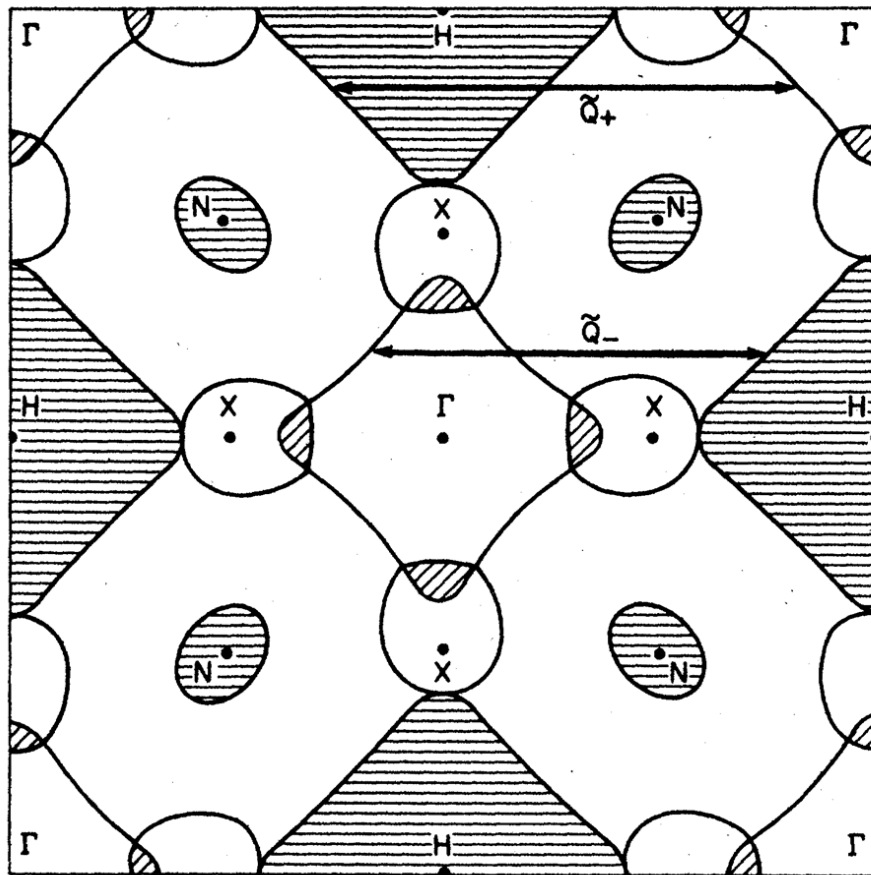


Figure 16: The Fermi surface of Chromium with the two nesting vectors labeled.

5.3 Previous Experimental Studies of Chromium

The first microscopic evidence for the SDW transition in chromium was discovered via neutron diffraction in 1953 where it was presented as an antiferromagnetic state with no definite explanation¹³. It was Overhauser in 1962 who first described this antiferromagnetic phase as a sinusoidal SDW state.

He further showed that there should be a gap in the band structure of chromium due to this phase transition and predicted it would have an energy $\sim 0.1\text{eV}$ ¹⁴. Barker was the first to observe this optical gap with energy of 0.12eV directly in 1969¹⁵. This was done using spectroscopic methods which are similar to the ones used in this experiment as discussed in section 2. Further spectroscopic investigation by Lind and Stanford however reported the existence of multiple gaps at infrared energies of 0.12 , 0.45 , and 0.9eV in chromium in 1972¹⁶. The most recent work done on identifying energy gaps due to the SDW was by Machida Lind and Stanford in 1984. They saw two gaps at 0.12 and 0.45eV which they associate with the SDW transition¹. Further a two gap model for the incommensurate SDW was put forth by Machida and Fujita in 1984 in which they were partially successful at predicting the temperature dependence of these gaps¹⁷. In the UV and visible range the optical constants have been found by Nestell and Christy² as well as by Romaniello *et. al.*³. For an in depth review into the past work done on chromium, both theoretical and experimental; please refer to Fawcett's comprehensive 1988 article⁶.

5.4 Discussion of Present Results

The chromium sample was purchased from Princeton Scientific. It is a disk with diameter 10mm and thickness 1mm . The agreement with past ellipsometry data along with the low surface roughness shown in figure 11 both seem to indicate that the chromium sample used was of good quality. This allows us to be confident in the quality of our reflectance and ellipsometry results.

There is however some slight discrepancy with past work in the 300K mid IR data which will prove important in our discussion. The prior work done on chromium at room temperature indicates that the gap near 3000 cm^{-1} has not yet closed all the way while ours has. Further the prior work states that the feature near 8000 cm^{-1} is still present at room temperature, whereas in our data this is not so clear. That the gap near 3000cm^{-1} is completely closed in our data while in theirs it is still open might imply that previously calculated temperature dependence are not correct. Further the attribution of the

feature at 8000cm^{-1} to the paramagnetic state no longer seems quite so evident, which would change the understanding of the SDW developed based on a two-gap model. However it should be seen in figure 12 that the signal to noise ratio above 7500cm^{-1} is $\sim 1\%$. This makes it difficult to say much more about this feature which is on the order of $\sim 2\%$. It would seem that more data should be taken on the temperature dependent reflectance of chromium at higher frequencies with near-infrared optics.

6 Conclusion and Outlook

In the past year we have built and tested a vacuum chamber for FTIR reflectance at high and low temperatures. Ultra-high vacuum has been achieved as well as temperatures ranging from 5-400K. A variety of pieces were designed, built, or tested including: An in situ gold evaporator, an external alignment assembly, an optical bread board, and UHV compatible IR windows. This new apparatus has been used to measure the IR reflectance of a variety of materials including LAO, LSMO, quartz, VO_2 and chromium. The chromium data has been compared with past results. While there is good agreement across the board the interpretation of the data is open to debate.

In our data it seems possible that a feature in the reflectance at 8000cm^{-1} disappears near the transition temperature of chromium, whereas previously it has been reported that this is not the case. It was argued on the grounds that this feature does not disappear above T_N that one should not associate it with the SDW transition in chromium. However, in light of our experiments we think this is still open to discussion. Further testing of the temperature dependence of the reflectance of chromium in the near IR and visible light ranges should be done to examine this further.

Works Cited

- [1] K. Machida, M. A. Lind, and J. L. Stanford, *Temperature Dependence of Infrared Reflectivity of Chromium -- Realization of Soliton Lattice Structure of Spin Density Wave*, J Phys Soc Jpn **53**, 11, 4020-4028 (1984).
- [2] J. E. Nestell Jr. and R. W. Christy, *Optical conductivity of bcc transition metals: V, Nb, Ta, Cr, Mo, W*, Phys Rev B **21**, 8, 3173-3179 (1980).
- [3] Romaniello *et. al.*, *Optical properties of bcc transition metals in the range 0–40 eV*, Phys Rev B **73**, 76, (2006)
- [4] Wooten, *Optical Properties of Solids*, 1st ed. (Academic Press, NY, 1972)
- [5] Trinity College Dublin, *Ellipsometry*, WWW Document, (<http://www.tcd.ie/Physics/Surfaces/ellipsometry2.php>).
- [6] Timoshenko and Woinowsky-Krieger, *Theory of Plates and Shells*, 2nd ed. (McGraw-Hill, NY, 1959).
- [7] Weissler and Carlson, *Methods in Experimental Physics Vol. 14- Vacuum Physics and Technology*, 1st ed. (Academic Press, NY, 1979)
- [8] E. Fawcett, *Spin-density-wave antiferromagnetism in chromium*, Rev. Mod. Phys. **60**, 1, 209-283 (1988)
- [9] Ashcroft and Mermin, *Solid State Physics*, 1st ed. (Holt, Rinehardt, and Winston, 1976).
- [10] G. Grüner, *Density Waves in Solids*, 1st ed. (Perseus Publishing, MA, 2000)
- [11] W. M. Lomer, *Electronic Structure of Chromium Group Metals*, Proc. Phys. Soc. **80**, 489 (1962)
- [12] A. S. Barker, Jr. and J. A. Ditzenberger, *Optical Studies of Antiferromagnetism in Chromium and Its Alloys*, Phys. Rev. B **1**, 11, 4378-4400 (1970)
- [13] C. G. Shull and M.K. Wilkinson, *Neutron Diffraction Studies of Various Transition Elements*, Rev. Mod. Phys. **25**, 1, 100-107 (1953)
- [14] A. W. Overhauser, *Spin Density Waves in an Electron Gas*, Phys. Rev. **128**, 3, 1437-1452 (1962)
- [15] A. S. Barker Jr., B. I. Halperin, T. M. Rice, *Antiferromagnetic Energy Gap in Chromium*, Phys. Rev. Lett. **20**, 8, 384-387 (1969)
- [16] M. A. Lind and J. L. Stanford, *Optical measurements of the antiferromagnetic energy gaps in Chromium*, Phys. Lett. A. **39**, 1, 5-6 (1972)
- [17] K. Machida and M. Fujita, *Soliton Lattice Structure of Incommensurate Spin Density Waves*, Phys. Rev. B. **30**, 9, 5284-5299 (1994)